Ruthenium Catalysts on Zr-SBA-15 and Nb/Zr-SBA-15 Supports for Xylose Hydrogenation

Viktor A. Golubkov, Yulia N. Zaitseva, Valentin V. Sychev, Anna O. Eremina, Sergei D. Kirik, Svetlana A. Novikova, Kseniya A. Litvintseva and Oxana P. Taran

Рутениевые катализаторы гидрирования ксилозы на носителях Zr-SBA-15 и Nb/Zr-SBA-15

В. А. Голубков, Ю. Н. Зайцева, В. В. Сычев, А. О. Еремина, С. Д. Кирик, С. А. Новикова,К. А. Литвинцева, О. П. Таран

Material and methods

Synthesis of supports and catalysts

Synthesis of 5Zr-SBA-15 support with ZrO_2 content 5 wt.% was carried out by co-precipitation according to the modified methodology [1]. The molar ratio of the reagents was 0.017 P123: 1.0 TEOS: 0.05 $ZrOCl_2$ * 8H_2O: 221.0 H_2O: 1.0 NaCl. Pluronic P123 was dissolved at room temperature in distilled water, and NaCl was added. Then stirred vigorously at 35 °C for 2 h, followed by the addition of zirconium source, $ZrOCl_2$. After 3 h after the addition of $ZrOCl_2$, TEOS was injected dropwise and stirred at 35 °C for 24 h. Hydrothermal treatment was carried out at 80 °C for 24 h. At the end of hydrothermal treatment, the material was filtered and washed with water to neutral. The precipitate was air dried for 2 days, followed by drying at 80 °C for 12 h. The structuring agent was removed by calcination at 550 °C for 12 h (temperature rise rate 1 °C/min).

For the synthesis of composites with niobium oxide, the method of impregnation by moisture capacity was carried out [2] using niobium oxalate in 0.1 M oxalic acid. The sample was then air dried at room temperature for 12 h and at 80 °C for 8 h. It was then calcined at 450 °C for 4 h (2 °C/min). The resulting material containing 10.0 wt% niobium oxide was designated as 10Nb/5Zr-SBA-15.

Ruthenium deposition was carried out by the incipient wetness impregnation method (IWI) using aqueous solution of $Ru(NO)(NO_3)_3$. The reduction was carried out in a flow of H_2 (200 mL/min), at 300 °C (1 °C/min) for 2 h. The catalyst then was passivated with 1 % O_2 in Ar [3]. For all the catalysts, the nominal loading of Ru 2 wt% was used. The catalysts were designated xRu/support, where the x is the Ru content in wt%.

Study of supports and catalysts

The acidic properties were studied by IR spectroscopy using pyridine as a probe molecule. The spectra were recorded on an IRTracer-100 FTIR spectrometer (Shimadzu, Japan) in the range of 1350–4000 cm^{-1} with a resolution of 4 cm^{-1}. The sample was calcined in vacuum in an IR cuvette for 1 h at 500 °C and cooled. Pyridine adsorption was carried out at 150 °C for 20 min, then desorbed at 150

or 300 C by vacuuming for 30 min. The concentrations of Brensted and Lewis acid centers (BAS and LAS, respectively) were determined from the integrated intensities of characteristic absorption bands [4, 5].

The morphology was studied on a Hitachi Regulus SU 8230 FE-SEM scanning electron microscope (Japan) with an accelerating voltage of 5–30 kV. The samples were deposited on holey carbon substrates on copper grids. The structure and microstructure were studied by high-resolution transmission electron microscopy (HRTEM) using a ThemisZ microscope (Thermo Fisher Scientific, USA) with a Ceta 16 CCD array, an accelerating voltage of 200 kV, and a resolution limit of 0.07 nm. The instrument is equipped with a SuperX energy-dispersive X-ray characteristic emission (EDX) spectrometer (Thermo Fisher Scientific, USA) with a semiconductor Si detector with an energy resolution of 128 eV. Microphotographs were processed in ImageJ software [20].

XPS studies were carried out on a SPECS X-ray photoelectron spectrometer (Germany) using MgK radiation (1253.6 eV). The binding energy scale ($E_{св}$) was calibrated using the $Au4f_{7/2}$ (84.00 eV) and $Cu2p_{3/2}$ (932.67 eV) lines, the Si2p (103.5 eV) line was used as an internal standard. The samples were applied on double-sided copper conductive tape. Recording at a transmission energy of 20 eV.

Diffuse reflectance spectra in the visible and ultraviolet regions (UV–Vis DRS) were recorded using a Shimadzu 3600 scanning spectrophotometer and an ISR-603 Integrating Sphere Attachment, spectral slit width 12 nm. The baseline was recorded relative to ultrapure barium(II) sulfate $BaSO_4$. The reflectance spectra were transformed using the Kubelka-Munk function. A separate region of the spectrum of ruthenium containing samples (350–450 nm) was processed by subtracting the baseline (straight line from the outermost arms of the absorption bands) and decomposing the spectra into individual absorption bands (Gaussian functions).

Studies by the temperature-programmed reduction method were carried out on a ChemBET Pulsar TPR/TPD (Quantachrome Inst., USA). The samples were dried in helium flow at T = 130 °C for 30 min. TPD profiles were recorded in a flow of a mixture of 10 %H_2 in Ar in the temperature range from 30 °C to 900 °C. The heating rate was 10 °C/min. The profiles were normalized to mass.

Textural properties of samples were studied by low-temperature nitrogen adsorption-desorption method on the analyzer ASAP 2420 (Micromeritics). Pre-degassing of the samples was carried out at 350 °C for 8 h at P $7–10^{-6}$ Pa. Specific surface area (S_{BET}) was calculated by BET method with correction by Ruckerol plot [6]. The pore volume was determined by the SinglePoint method at P/P_0 = 0.995. Pore size distribution was determined by the BJH-KJS method, mesopore diameter (D) by the maximum of the distribution. The wall thickness was determined as the difference between the cell parameter and the pore diameter.

Powder diffraction data were obtained on an X'Pert PRO diffractometer with a PIXcel detector (PANalytical) with a graphite monochromator and CuKα radiation. Patterns were taken in the low-angle range from 0.5 to 5° on the 2θ scale, step 0.026°, Δt – 200 s. In the far-angle region from 3 to 80° 2θ, step 0.026°, Δt – 50 s. The cell parameter was calculated from the interplanar distance of the reflex $(100) a = \left(2/\sqrt{3} * d_{100}\right)$.

Catalytic tests in the hydrogenation of xylose were carried out in a 100 mL AutoclaveEngineers (USA) autoclave reactor made of Hastelloy C 276. 0.3 g of xylose (Panreac, Pharm.), 0.1 g of catalyst, and 0.03 L of water were loaded. The reaction was carried out at 70 °C, 5.5 MPa H_2, 1200 rpm. Quantitative analysis of xylose and xylitol was performed on an Agilent 1260 Infinity II HPLC, Rezex RPM–Monosaccharide Pb column^{2+} 300 × 7.8 mm, refractometric detection, eluent was

deionized water, 70 °C, 0.6 mL/min. Qualitative analysis was performed using an Agilent 7890A gas chromatograph with an Agilent 7000A quadrupole mass detector, HP-5ms 30 m × 0.25 mm × 0.25 mm capillary column; pre-derivatization (silanization) in a mixture of trimethylchlorosilane and hexamethyldisilazane in pyridine medium [21].

Results and Discussion

XPS data

In the XPS spectra of supports and catalysts, the Si*2p* binding energy is 103.5 eV, which is a characteristic value for Si^{4+} within SiO_2 [7]. The O*1s* line has a binding energy of ~ 532.9 eV, typical for silicon oxide in SBA-15 [7], for the 10Nb/5Zr-SBA-15 sample, a shoulder around 531 eV is observed for oxygen in niobium oxide [8]. The binding energy of Zr$3d_{5/2}$ is 183.4±0.1 eV, which is characteristic of the Zr^{4+} state and close to zirconium in the ZrO_2 in structure SBA-15 [9], possibly in a structure close to $ZrSiO_4$ [10]. The binding energy of Nb$3d_{5/2}$ is 208.0±0.1 eV, which is higher than that of massive Nb_2O_5 (207.6) [11], and corresponds to Nb^{5+} in oxides bound to SiO_2 [12].

Table S1. Atomic ratios of elements in the near-surface layer of the atomic ratios of elements in the near-surface layer of samples according to XPS data.

Sample		5Zr-SBA-15	10Nb/5Zr-SBA-15	2Ru/5Zr-SBA-15	2Ru/10Nb/5Zr-SBA-15
Atomic fractions of elements, at.%	Si	25.5	22.4	27.9	22.4
	Zr	2.2	0.7	1.0	0.6
	Nb	-	0.7	-	0.6
	Ru	-	-	0.3	0.2
Fractions of ruthenium in different states, at.%	Ru^0	-	-	20.0	0
	RuO_2	-	-	56.0	100.0
	RuO_3	-	-	24.0	0

Diffuse reflectance Uv-vis spectroscopy

Diffuse reflectance Uv-vis spectroscopy shows a fundamentally different pattern in the distribution of ruthenium states in the catalysts (Fig. S1).

In the diffuse reflectance spectra, the supports have only one absorption band with a maximum at 270–290 nm, the differences between the support spectra of 5Zr-SBA-15 and 10Nb/5Zr-SBA-15 are insignificant, there is a bathochromic shift upon deposition of niobium oxide. The main absorption band with a maximum at 270–290 nm refers to the charge transfer from ligand to metal (O^{2-}, OH^- and $OH_2 \rightarrow Si^{4+}$, Zr^{4+}, Nb^{5+}) in oxides [13, 14]. Amorphous SiO_2 in SBA-15 matrix absorbs light starting at 350 nm [15]. Massive Nb_2O_5 has strong absorption even above 400 nm [16, 17], and ZrO_2 – up to 350 nm [18, 19]. The absence of such support absorption bands indicates the absence of separate massive Nb and Zr oxides and their incorporation into the silicate matrix of SBA-15.

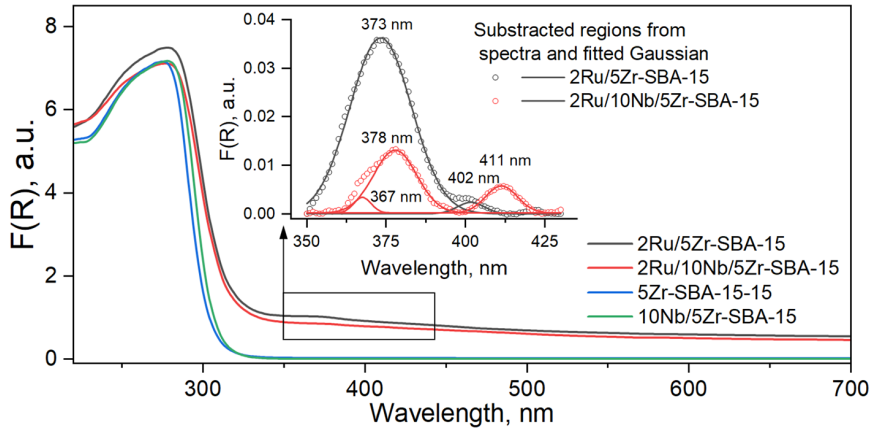

Fig. S1. Diffuse reflectance spectra of supports and catalysts

Microscopy and N 2 adsorption-desorption

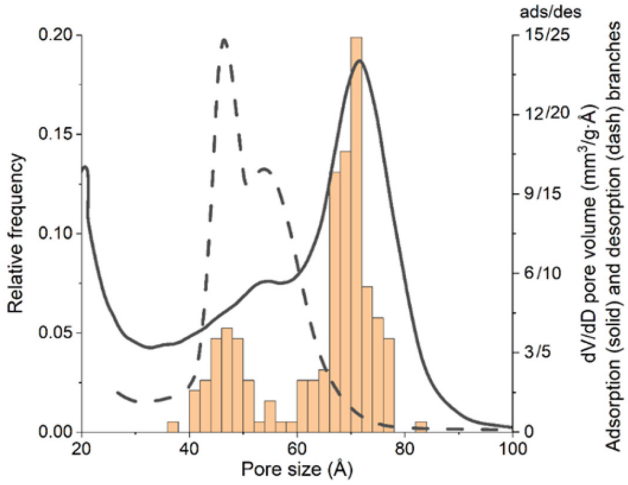

Fig. S3. Mesopore size distributions of 2Ru/10Nb/5-Zr-SBA-15: columns – SEM, line – nitrogen adsorption-desorption

XRD in the region of high angles

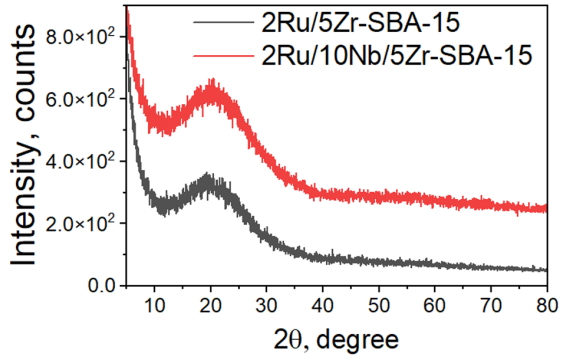

Fig. S4. Diffractograms in the region of high angles

References

[1] Thunyaratchatanon C., Luengnaruemitchai A., Chaisuwan T., Chollacoop N., Chen S.-Y., Yoshimura Y. Synthesis and characterization of Zr incorporation into highly ordered mesostructured SBA-15 material and its performance for CO_2 adsorption. *Microporous and Mesoporous Materials 2017.* Vol. 253, P. 18–28.

[2] García-Sancho C., Saboya R.M. A., Cecilia J.A., Sales A.V., Luna F.M. T., Rodríguez-Castellón E., Cavalcante C.L. Influence of pore size and loading for Nb_2O_5/SBA-15 catalysts on synthetic ester production from free fatty acids of castor oil. *Molecular Catalysis 2017.* Vol. 436, P. 267–275.

[3] Miroshnikova A. V., Sychev V.V., Tarabanko V.E., Kazachenko A.S., Skripnikov A.M., Eremina A.O., Kosivtsov Y., Taran O.P. Reductive Fractionation of Flax Shives in Ethanol Medium over RuNi Bimetallic Catalysts. *International Journal of Molecular Sciences 2023.* Vol. 24(14), P. 11337.

[4] Anderson J. A., Fergusson C.A. Surface and bulk properties of silica–zirconia mixed-oxides: acid vs base catalysed condensation. *Journal of non-crystalline solids 1999.* Vol. 246(3), P. 177–188.

[5] Anderson J. A., Fergusson C., Rodríguez-Ramos I., Guerrero-Ruiz A. Influence of Si/Zr ratio on the formation of surface acidity in silica-zirconia aerogels. *Journal of Catalysis 2000.* Vol. 192(2), P. 344–354.

[6] Rouquerol J., Llewellyn P., Rouquerol F. Is the BET equation applicable to microporous adsorbents. *Stud. Surf. Sci. Catal 2007.* Vol. 160(07), P. 49–56.

[7] Sychev V. V., Malyar Y.N., Skripnikov A.M., Trotsky Y.A., Zaitseva Y.N., Eremina A.O., Borovkova V.S., Taran O.P. Larix Sibirica Arabinogalactan Hydrolysis over Zr-SBA-15; Depolymerization Insight. *Molecules 2022*. Vol. 27(24), P. 8756.

[8] Usha N., Sivakumar R., Sanjeeviraja C., Arivanandhan M. Niobium pentoxide (Nb2O5) thin films: rf Power and substrate temperature induced changes in physical properties. *Optik-International Journal for Light and Electron Optics 2015*. Vol. 126(19), P. 1945–1950.

[9] Huo L., Wang T., Xuan K., Li L., Pu Y., Li C., Qiao C., Yang H., Bai Y. Synthesis of dimethyl carbonate from CO_2 and methanol over Zr-based catalysts with different chemical environments. *Catalysts 2021*. Vol. 11(6), P. 710.

[10] Jones D., Jiménez-Jiménez J., Jiménez-López A., Maireles-Torres P., Olivera-Pastor P., Rodriguez-Castellón E., Rozière J. Surface characterisation of zirconium-doped mesoporous silica. *Chemical Communications 1997*(5), P. 431–432.

[11] McGuire G., Schweitzer G.K., Carlson T.A. Core electron binding energies in some Group IIIA, VB, and VIB compounds. *Inorganic Chemistry 1973.* Vol. 12(10), P. 2450–2453.

[12] Sobczak I., Kozlowska M., Ziolek M. Au containing mesostructured cellular foams NbMCF and ZrMCF in selective oxidation of methanol to formaldehyde. *Journal of Molecular Catalysis A: Chemical 2014*. Vol. 390, P. 114–124.

[13] Gromov N. V., Taran O.P., Semeykina V.S., Danilova I.G., Pestunov A.V., Parkhomchuk E.V., Parmon V.N. Solid Acidic NbOx/ZrO2 Catalysts for Transformation of Cellulose to Glucose and 5-Hydroxymethylfurfural in Pure Hot Water. *Catalysis Letters 2017.* Vol. 147(6), P. 1485–1495.

[14] Gao X., Wachs I.E. Investigation of Surface Structures of Supported Vanadium Oxide Catalysts by UV-vis–NIR Diffuse Reflectance Spectroscopy. *The Journal of Physical Chemistry B 2000*. Vol. 104(6), P. 1261–1268.

[15] Scheinost A. C., Ford R. G., Sparks D. L. The role of Al in the formation of secondary Ni precipitates on pyrophyllite, gibbsite, talc, and amorphous silica: a DRS study. *Geochimica et Cosmochimica Acta 1999.* Vol. 63(19–20), P. 3193–3203.

[16] Habibi M., Mokhtari R. First Observation on S-doped Nb2O5 Nanostructure Thin Film Coated on Carbon Fiber Paper Using Sol–Gel Dip-Coating: Fabrication, Characterization, Visible Light Sensitization, and Electrochemical Properties. *Journal of Inorganic and Organometallic Polymers and Materials 2011.* Vol. 22.

[17] Scotti N., Ravasio N., Evangelisti C., Psaro R., Penso M., Niphadkar P. S., Bokade V. V., Guidotti M. Epoxidation of Karanja (Millettia pinnata) Oil Methyl Esters in the Presence of Hydrogen Peroxide over a Simple Niobium-Containing Catalyst. *Catalysts 2019.* Vol. 9(4), P. 344.

[18] Ranga Rao G., Sahu H. R. XRD and UV–Vis diffuse reflectance analysis of CeO 2-ZrO 2 solid solutions synthesized by combustion method. *Journal of chemical sciences 2001.* Vol. 113, P. 651–658.

[19] Olvera Olmedo O. G., Díaz de León Hernández J. N., Suárez-Toriello V. A., Reyes Heredia J. A. d.l. Effect of the Structural and Electronic Properties of Rh/CeXZr1-XO2 Catalysts on the Low-temperature Ethanol Steam-reforming. *Journal of the Mexican Chemical Society 2021.* Vol. 65(1), P. 20–38.